Inorganic Chemistry

Article

pubs.acs.org/IC

Cis−Trans Interconversion in Ruthenium(II) Bipyridine Complexes

Yeraldith Rojas Pérez, Leonardo D. Slep,* and Roberto Etchenique*

Departamento de Química Inorgánica, Analítica y Química Física, INQUIMAE, Facultad de Ciencias Exactas y Naturales, Universidad de Buenos Aires, Pabellón 2, Ciudad Universitaria, C1428EHA Buenos Aires, Argentina

Supporting Information

ABSTRACT: Most studies of ruthenium polypyridine complexes are devoted to their *cis* isomers. The fact that *cis* isomers are thermally more stable and thus easier to synthesize has prevented researchers from investigating the properties and applications of *trans* complexes. We present a study of thermal and photochemical *cis*−*trans* interconversion of the key complex $[Ru(bpy)_2(PMe_3)(H_2O)]^{2+}$ (bpy = 2,2′-bipyridine, PMe_3 = trimethylphosphine), which results in specific synthetic applications of the trans species, potentially useful as a platform for designing highly efficient visible light activated caged compounds. We show, as a proof of concept, some examples of trans complexes bearing N-donor and P-donor ligands and their comparison with the cis isomers.

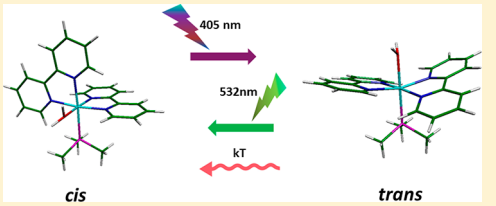

INTRODUCTION

Ruthenium bipyridine complexes have been profusely studied. They present a rich and interesting photochemistry that arises from a strong Ru(II) → π^*_{bpy} MLCT absorption band followed by the thermal population of a nearby ^{3}d−d dissociative state after being irradiated. This state lasts long enough to undergo photochemical reactions, usually expelling monodentate ligands and leaving a $[Ru(bpy)_2(Solvento)]$ species.[1]

These characteristics have been employed in photochemical synthesis[2] and also in the design of visible light activatable caged compounds. The first caged compound based on $\{Ru(bpy)_2\}^{2+}$ chemistry[3] was *cis*-$[Ru(bpy)_2(4AP)_2]^{2+}$, a complex that delivers 4-aminopyridine (4AP), a blocker of K^+ channels,[4] either in a linear regime under irradiation with blue light or in a two-photon regime when NIR light is used.[5]

Many other phototriggers based on Ru-bpy complexes have been subsequently reported, including caged glutamate,[6] γ-aminobutyric acid,[7] nicotine,[8] serotonine,[9] dopamine,[10] and biomedically relevant nitriles.[11] A similar approach, although based on a different chemistry, has been employed to devise nitric oxide deliverers.[12]

Relevant theoretical studies of this family of complexes have also been reported,[13] all of them devoted to the thermally more favorable *cis* form, while just a few works report calculated data of the trans isomers, for the diaquo *trans*-$[Ru(bpy)_2(H_2O)_2]^{2+}$ [14] or the light harvesting related complex *trans*-$[Ru(dcbpy)_2(NCS)_2]$[15] (dcbpy = 4,4′-dicarboxy-2,2′-bipyridine).

In this work we present a study of the photochemical interconversion between *cis*- and *trans*-$[Ru(bpy)_2(PMe_3)(H_2O)]^{2+}$, showing that the *trans* aquo isomer can be regarded as a useful platform to devise new highly efficient $[Ru(bpy)_2(PMe_3)L]^{n+}$ phototriggers with a *trans* conformation.

EXPERIMENTAL SECTION

Syntheses. All procedures were done under Argon.

cis-$[Ru(bpy)_2(PMe_3)Cl)]Cl$ was obtained as described elsewhere.[16]

trans-[Ru(bpy)$_2$(PMe$_3$)(H$_2$O)](CF$_3$SO$_3$)$_2$ ([1](CF$_3$SO$_3$)$_2$). A 100 mg portion of *cis*-$[Ru(bpy)_2(PMe_3)Cl)]Cl$ was dissolved in 3.0 mL of distilled water. The solution was stirred with 500 mg of Dowex-22 anionic resin previously loaded with mesylate ion. Aquation of the complex proceeds simultaneously with the ion exchange step, yielding *cis*-$[Ru(bpy)_2(PMe_3)(H_2O)](CH_3SO_3)_2$. The obtained solution was filtered and diluted to 20 mM, and 5 equiv of trifluoromethanesulfonic acid was added. The mixture was put into an ice bath and irradiated with a 150 W metal halide lamp for 3.5 h. After 30 min of irradiation the complex $[\mathbf{1}](\mathbf{CF_3SO_3})_2$ began to precipitate from the mixture. It was filtered and washed with portions of 0.1 M KPF_6 until pH >4, further washed with *tert*-butyl alcohol, and vacuum-dried. An intense red crystalline solid was obtained. Yield: 42%. ε_{max}(460 nm) = 9.7×10^3 M^{-1} cm^{-1}. ^{1}H NMR (500 MHz, D_2O/acetone-d_6): δ (ppm) 9.30 (4H, d, 5.46 Hz); 8.47 (4H, d, 8.36 Hz); 8.19 (4H, t, 7.86 Hz); 7.73 (4H, t, 6.87 Hz); 0.574 (9H, d, 9.99 Hz) (see Figure S1) MS (ESI$^+$): *m*/*z* 639.0417 $[[\mathbf{1}] - H_2O + CF_3SO_3]^+$; 254.0459 $[\mathbf{1}]^{2+}$; 245.0444 $[[\mathbf{1}] - H_2O]^{2+}$; 216.0273 $[[\mathbf{1}] - PMe_3]^{2+}$; 207.0218 $[[\mathbf{1}] - H_2O - PMe_3]^{2+}$ (see Table S1, Figure S2).

cis-[Ru(bpy)$_2$(PMe$_3$)(H$_2$O)](CF$_3$SO$_3$)$_2$ ([2](CF$_3$SO$_3$)$_2$). A 50 mg portion of $[\mathbf{1}](\mathbf{CF_3SO_3})_2$ was dispersed in 3.0 mL of distilled water. The mixture was heated to 60 °C under argon for 3 days and the obtained solution lyophilized. In case the mesylate salt was needed, a further ion exchange with Dowex-22 previously charged with $CH_3SO_3^-$ ion was performed to yield $[\mathbf{2}](\mathbf{CH_3SO_3})_2$. ε_{max}(444 nm) = 6.7×10^3 M^{-1} cm^{-1}. ^{1}H NMR (300 MHz, acetone-d_6): δ (ppm) 9.19 (1H, d, 5.79 Hz); 8.95 (1H, d, 5.50 Hz); 8.48 (1H, d, 8.16 Hz); 8.43 (1H, d, 8.08 Hz); 8.39 (1H, d, 8.25 Hz); 8.20 (1H, d, 8.25 Hz); 8.17 (1H, t, 8.25 Hz); 8.12 (1H, t, 8.25 Hz); 7.94 (1H, t, 7.83 Hz); 7.74 (4H, m); 7.46 (1H, s); 7.24 (1H, t, 6.58 Hz); 7.02 (1H, t, 6.76 Hz); 1.03 (9H, d, 8.89 Hz) (see Figure S3). MS (ESI$^+$): *m*/*z* 639.0388 $[[\mathbf{2}] - H_2O + CF_3SO_3]^+$; 245.0432 $[[\mathbf{2}] - H_2O]^{2+}$;

Received: May 21, 2019

DOI: 10.1021/acs.inorgchem.9b01485
Inorg. Chem. XXXX, XXX, XXX−XXX

216.0262 = $[[\mathbf{2}] - PMe_3]^{2+}$; 207.0208 $[[\mathbf{2}] - H_2O - PMe_3]^{2+}$ (see Table S2, Figure S4).

*cis-[Ru(bpy)$_2$(PMe$_3$)(ImH)](PF$_6$)$_2$ (**[3](PF$_6$)$_2$**).* A 90 mg portion of $[\mathbf{2}](\mathbf{CH_3SO_3})_2$ was dissolved in 3 mL of distilled water. A 73 mg portion of imidazole was added, and the mixture was stirred at 50 °C for 24 h and then cooled to room temperature and precipitated with 600 μL of aqueous KPF_6 0.5 M. An orange solid was obtained. It was filtered, washed with water several times, and vacuum-dried. Further purification was carried out by exchanging the PF_6 ion by chloride using Dowex-22 anionic resin and reprecipitating with KPF_6. Yield: 45%. ε_{max}(431 nm) = 6.0 × 10^3 M^{-1} cm^{-1}. ^{1}H NMR (500 MHz, D_2O/acetone-d_6): δ (ppm) 9.23 (1H, d, 5.45 Hz); 8.80 (1H, d, 8.35 Hz); 8.54 (1H, d, 7.35 Hz); 8.41 (1H, d, 7.85 Hz); 8.36 (1H, d, 8.10 Hz); 8.33 (1H, d, 8.35 Hz); 8.20 (1H, t, 7.85 Hz); 8.09 (1H, t, 7.97 Hz); 7.91 (1H, t, 7.97 Hz); 7.84 (1H, t, 7.97 Hz); 7.73 (3H, m); 7.51 (2H, s); 7.30 (1H, t, 6.43 Hz); 7.17 (1H, t, 6.78 Hz); 7.02 (1H, t, 1.42 Hz); 6.76 (1H, t, 1.48 Hz); 0.99 (9H, d, 8.42 Hz) (see Figure S5). MS (ESI$^+$): *m*/*z* 703.0878 $[[\mathbf{3}] + PF_6]^+$; 279.0632 $[\mathbf{3}]^{2+}$; 245.0444 $[[\mathbf{3}] - ImH]^{2+}$; 207.0221 $[[\mathbf{3}] - ImH - PMe_3]^{2+}$ (see Table S3, Figure S6).

*trans-[Ru(bpy)$_2$(PMe$_3$)(ImH)](PF$_6$)$_2$ (**[4](PF$_6$)$_2$**).* A 39 mg portion of $[\mathbf{1}](\mathbf{CF_3SO_3})_2$ was dissolved in 2 mL of dry MeOH. A 21 mg portion of imidazole was dissolved in 500 μL of dry MeOH and mixed with the previous solution. This mixture was stirred at 40 °C for 40 min and then cooled to 0 °C and precipitated by addition of 500 μL of aqueous KPF_6 0.5 M. The precipitate was filtered, washed two times with KPF_6 0.1 M and then with water, and dried under vacuum. Yield: 77%. ε_{max}(464 nm) = 8.9 × 10^3 M^{-1} cm^{-1}. ^{1}H NMR (300 MHz, acetone-d_6): δ (ppm) 9.81 (4H, d, 5.63 Hz); 8.67 (4H, d, 8.22 Hz); 8.33 (4H, t, 7.79 Hz); 7.94 (4H, t, 6.92 Hz); 7.43 (1H, s), 7.00 (1H, s); 6.47 (1H, s); 0.80 (9H, d, 9.30 Hz) (see Figure S7). MS (ESI$^+$): *m*/*z* 703.0875 $[[\mathbf{4}] + PF_6]^+$; 279.0617 $[\mathbf{4}]^{2+}$; 245.0430 $[[\mathbf{4}] - ImH]^{2+}$; 207.0207 $[[\mathbf{4}] - ImH - PMe_3]^{2+}$ (see Table S4, Figure S8).

*trans-[Ru(bpy)$_2$(PMe$_3$)(PPh$_3$)](PF$_6$)$_2$ (**[5](PF$_6$)$_2$**).* A 64 mg portion of $[\mathbf{1}](\mathbf{CF_3SO_3})_2$ was dissolved in 2 mL of dry MeOH. A 206 mg portion of PPh_3 (PPh_3 = triphenylphosphine) were dissolved in 2 mL of dry MeOH and mixed with the previous solution. This mixture was stirred at 50 °C for 3 h and then cooled to 0 °C. The excess PPh_3 was separated, and 5 equiv of KPF_6 was added. The orange solid was filtered, washed with MeOH and diethyl ether, and dried under vacuum. Yield: 48%. ε_{max}(440 nm) = 10.2 × 10^3 M^{-1} cm^{-1}. ^{1}H NMR (300 MHz, acetone-d_6): δ (ppm) 9.29 (4H, d, 5.65 Hz); 8.58 (4H, d, 8.00 Hz); 8.32 (4H, t, 8.00 Hz); 7.80 (4H, t, 5.63 Hz); 7.40 (3H, t, 7.55 Hz); 7.16 (6H, t, 7.32 Hz); 6.41 (6H, t, 8.46 Hz); 0.55 (9H, dd, 9.40 Hz) (see Figure S9). MS (ESI$^+$): *m*/*z* 376.0892 $[\mathbf{5}]^{2+}$; 338.0668 $[[\mathbf{5}] - PMe_3]^{2+}$; 245.0430 $[[\mathbf{5}] - PPh_3]^{2+}$; 207.0206 $[[\mathbf{5}] - PMe_3 - PPh_3]^{2+}$ (see Table S5, Figure S10).

*trans-[Ru(bpy)$_2$(PMe$_3$)$_2$](PF$_6$)$_2$ (**[6](PF$_6$)$_2$**).* A 95 mg portion of $[\mathbf{1}](\mathbf{CF_3SO_3})_2$ was dissolved in 2 mL of dry MeOH. A 400 μL portion of a 1 M PMe_3 solution in THF was added, yielding an immediate color change of the solution. After 2 h of stirring at room temperature, the reaction mixture was cooled to 0 °C and 500 μL of 0.5 M aqueous solution of KPF_6 was added. The orange precipitate was collected by filtration and washed three times with a 1/1 water/MeOH mixture and once with diethyl ether. Yield: 89%. ε_{max}(445 nm) = 10.2 × 10^3 M^{-1} cm^{-1}. ^{1}H NMR (300 MHz, acetone-d_6): δ (ppm) 9.66 (4H, d, 5.60 Hz); 8.82 (4H, d, 8.04 Hz); 8.40 (4H, t, 7.86 Hz); 7.97 (4H, t, 6.50 Hz); 0.65 (18H, t, 3.34 Hz) (see Figure S11). MS (ESI$^+$): *m*/*z* 283.0651 $[\mathbf{6}]^{2+}$; 245.0450 $[[\mathbf{6}] - PMe_3]^{2+}$; 207.0231 $[\mathbf{6}] - 2PMe_3]^{2+}$ (see Table S6, Figure S12).

Spectroscopic Measurements and Photolysis. The optical bench used for UV−vis measurements consisted of a 532 nm, 10 mW DPSS laser or 405 nm, 45 mW laser diode, collimated and directed toward a four-faceted cuvette, kept at 25 °C; the sample tested was stirred. The absorbance was monitored perpendicularly to the laser path using an OceanOptics PC2000 CCD spectrophotometer run by OOIChem sofware.

Quantum yield measurements of photouncaging were performed by recording the spectra while the photoreaction occurred under a calibrated laser source. Then, the quantum yield of photolysis was adjusted as a parameter in order to fit the corresponding equations.

NMR spectra were obtained with Bruker AM-500, Bruker Advance Neo 500, and Bruker Fourier 300 spectrometers. Internal standard NMR ^{1}H (standard EtOH) measurements were performed to obtain molar absorptivity values. All molar absorptivity values are given in aqueous solution. Samples for mass spectrometric measurements were prepared in LC-MS quality methanol and were performed by straight injection of the samples into the spectrometer, equipped with an ionization electrospray (ESI) source and using a high-resolution and high-accuracy hybrid quadrupole (Q) and orthogonal time of flight (Tof) mass spectrometer and Xevo G2S Q-TOF (Waters Corp.) operating in the positive ion mode. Typically, the cations were detected as the naked doubly charged gaseous species but also via a series of cations with reduced charge states achieved via ion pairing. In every case, only the observed *m*/*z* value of the most abundant isotopologue ion of the multi-isotopic species forming multifaceted isotope clusters is mentioned.

Theoretical Computations. Density functional theory (DFT) was employed to fully optimize the ground and lowest energy triplet-state geometries of *cis*- and *trans*-$[Ru(bpy)_2(PMe_3)(H_2O)]^{2+}$. The calculations were performed with Gaussian 09[17] using Becke's three-parameter hybrid functional with the correlation functional of Lee, Yang, and Parr formalized as the B3LYP hybrid functional[18] and the effective core potential basis set LanL2DZ implemented in G09,[17] which describes first-row elements using Dunning's D95V basis set and the Los Alamos ECP plus DZ basis for the heavier elements.[19] This combination proved to be suitable for electronic structure computations, geometry predictions, and spectral assignment in coordination compounds related to those described in this report.[12c,20] Tight SCF convergence criteria and no symmetry constraints were used along the geometry optimizations. The polarizable continuum model (PCM) approximation was used all along the computations to account for solvation effects in water. Coordinated H_2O might engage in specific solute−solvent interactions. No improvement in the computed (TD)DFT electronic spectra (vide infra) was observed upon inclusion of discrete explicit water molecules in the computations. While this strategy proved necessary in other situations,[20a,21] it was avoided here to reduce the computational cost. The nature of the stationary points obtained in the optimization procedures was checked by means of vibrational analyses. Electronic spectra for the different species were computed by (TD)DFT, involving at least 100 excited states at the same level of theory as that employed in the minimization step.

Energy profiles calculated for the electronic ground state as well as for the low-lying triplet excited states provide a microscopic description of the lowest energy reaction pathway. Taking into account that the exchange of ligands in ruthenium octahedral complexes usually proceeds via a dissociative pathway, the elongation coordinate of the Ru−O bond in *cis*-/*trans*-$[Ru(bpy)_2(PMe_3)(H_2O)]^{2+}$ was explored. The pentacoordinated species *cis*-/*trans*-$[Ru(bpy)_2(PMe_3)]^{2+}$ derived from the complete dissociation of an H_2O molecule were fully optimized as both singlet and triplet species. Transition state geometries associated with the *cis*- to *trans*-$[Ru(bpy)_2(PMe_3)]^{2+}$ interconnection were identified and optimized. The synchronous transit-guided quasi-Newton (STQN) method[22] implemented in G09 was used for this purpose. The vibrational analyses of the species optimized in this way showed a single imaginary frequency, consistent with a first-order saddle point on the potential energy surface (PES). The reaction coordinate linking the TS with the pentacoordinated *cis*-/*trans*-$[Ru(bpy)_2(PMe_3)]^{2+}$ local minima in both the ground and excited state's PES was revealed by Fukui's intrinsic reaction coordinate (IRC) computations.[23]

RESULTS AND DISCUSSION

It is known that refluxing the complex $[Ru(bpy)_2Cl_2]$ in water/EtOH mixtures makes it possible to obtain the mono and bis aqua complexes $[Ru(bpy)_2Cl(H_2O)]^+$ and $[Ru(bpy)_2(H_2O)_2]^{2+}$, both in a *cis* configuration.[1,2] Durham et

DOI: 10.1021/acs.inorgchem.9b01485
Inorg. Chem. XXXX, XXX, XXX−XXX

al. showed that *trans*-$[Ru(bpy)_2(H_2O)_2]^{2+}$ can be photochemically prepared[24] by irradiation of a solution of the *cis* isomer in the presence of a suitable anion that might induce the fractional precipitation of the *trans* form, leaving the unreacted *cis* precursor in solution. This *trans* species spontaneously reverts to the *cis* form in solution. Although it can be used to perform some further reactions,[25] its lifetime in aqueous solution at moderate temperatures is in the tens of minutes, preventing its use in most syntheses.

If the electron-acceptor ligand PMe_3 is introduced, the lability of the resulting complex toward ligand exchange is reduced. The same trend occurs regarding *cis*–*trans* thermal isomerization. By irradiation of a solution of *cis*-$[Ru(bpy)_2(PMe_3)(H_2O)]^{2+}$ in the presence of triflate ions, a precipitate of pure *trans*-$[Ru(bpy)_2(PMe_3)(H_2O)]^{2+}$ is obtained. The characteristic four aromatic signals of the NMR spectrum (Figure 1) unequivocally confirms the trans nature of

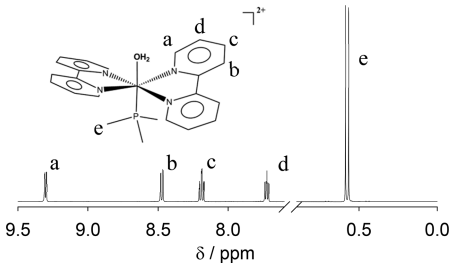

Figure 1. Structure and ^1H NMR spectrum of *trans*-$[Ru(bpy)_2(PMe_3)(H_2O)]^{2+}$ in D_2O.

this complex. Even when this species eventually undergoes thermal *trans*–*cis* isomerization as do other $\{Ru(bpy)_2\}^{2+}$ complexes, it can be stored for long periods in solid form. It is stable enough in aqueous solutions to perform proper characterization, and most interestingly it can be warmed in the presence of other ligands for synthetic purposes.

Photochemical Properties. A comparison between both isomers shows a red-shifted MLCT band with a higher absorptivity for the trans form (ε_{max} = 9.7 × 10^3 M^{-1} cm^{-1} at 460 nm vs ε_{max} = 6.7 × 10^3 M^{-1} cm^{-1} at 444 nm, see Supporting Information, Figures S13 and S14), which suggests a quality that makes it attractive for the design of a platform of long-wavelength-active caged compounds. Irradiation of a solution containing pure *trans* isomer shows that this form is also photoactive, undergoing reverse isomerization to the *cis* form. A simple mechanistic model can be used to elucidate the main parameters that govern the photoactivity:

$$cis\text{-}[Ru(bpy)_2(PMe_3)(H_2O)]^{2+} \underset{k}{\overset{\varphi_1}{\underset{\varphi_2}{\rightleftharpoons}}} trans\text{-}[Ru(bpy)_2(PMe_3)(H_2O)]^{2+}$$

where φ_1 and φ_2 are the isomerization quantum yields and k the kinetic constant of the *trans*/*cis* thermal isomerization. Therefore

$$\frac{d[cis]}{dt} = k[trans] + I_0(1 - 10^{-\varepsilon_t l[trans]}) - I_0(1 - 10^{-\varepsilon_c l[cis]}) \quad (1)$$

where I_0 is the irradiation power, ε_t and ε_c are the molar absorptivities of the *trans* and *cis* forms at the irradiation wavelength, respectively, and l is the optical path length. At T ≅ 25 °C and high irradiation intensities, k can be regarded as negligible. On the other hand, for low absorbances at the irradiation wavelength and 1 cm path length, the differential equation can be linearized. Under this condition

$$\frac{d[cis]}{dt} = 2.3 I_0 l(\varepsilon_t[trans] - \varepsilon_c[cis]) \quad (2)$$

The integration of the latter equation yields a monoexponential of the general form

$$[trans] = A(1 - e^{-kt}) + B \quad k = \frac{2.3 I_0}{V}(\varepsilon_c\phi_c + \varepsilon_t\phi_t) \quad (3)$$

where V is the reaction volume of the cuvette and ϕ_c and ϕ_t are the quantum efficiencies of isomerization for the direct and inverse photoreactions, respectively.

Due to the fact that the photoisomerization proceeds in both *cis* to *trans* and *trans* to *cis* ways, irradiation of *cis*- or *trans*-$[Ru(bpy)_2(PMe_3)(H_2O)]^{2+}$ solutions always yields an isomeric mixture. In the photostationary steady state the [*cis*]/[*trans*] ratio is given by the quotient $\phi_t\varepsilon_t/\phi_c\varepsilon_c$.

Figure 2 shows a typical photolysis experiment of *trans*-$[Ru(bpy)_2(PMe_3)(H_2O)]^{2+}$ in a UV–vis cuvette using a 532

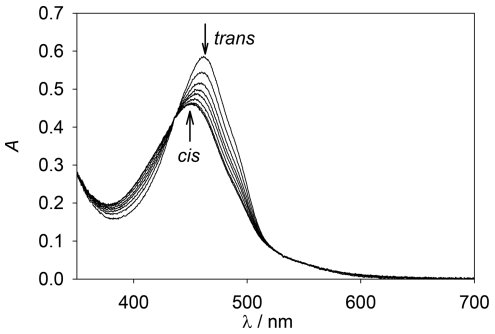

Figure 2. UV–vis spectra taken during photolysis of *trans*-$[Ru(bpy)_2(PMe_3)(H_2O)]^{2+}$ in water using a 532 nm laser.

nm laser. The presence of an isosbestic point indicates that just two colored species are present, as expected. Full spectrum analysis of the product using pure *cis* and *trans* complexes as standards shows a [*cis*]/[*trans*] ratio of 2.08 in the photostationary state. As ε_t and ε_c can be measured from the pure complexes, it is possible to determine that ϕ_t is 1.5 times higher than ϕ_c. This result is at least striking, considering the fact that a totally opposite trend has been reported when the photosubstitution processes in the related *cis*-$[Ru(bpy)_2XY]^{n+}$ species have been studied.[1] By fitting the complete photolysis to eq 3, it is possible to obtain the values ϕ_t = 0.158 and ϕ_c = 0.105, respectively. It is important to note that full photolysis of the *trans* isomer does not yield a pure *cis* species but a photostationary state. Figure 3 shows the spectra of the pure species and the different photostationary states that can be established by changing the irradiation wavelength. Due to its bathochromic shift, the *trans* species is less absorptive at short wavelengths (405 nm) and a higher molar fraction of this isomer is obtained. Conversely, the *cis* form predominates under irradiation at 532 nm.

Thermal Interconversion. The thermal decay of the *trans* form to its *cis* isomer is another key feature in order to evaluate synthetic potentiallity. The half-life in aqueous solution ranges from 14 h at 30 °C to about 30 min at 60 °C, long enough to obtain reasonably pure *trans* complexes by ligand exchange (vide infra). An Eyring plot of the thermal decay (see

DOI: 10.1021/acs.inorgchem.9b01485
Inorg. Chem. XXXX, XXX, XXX–XXX

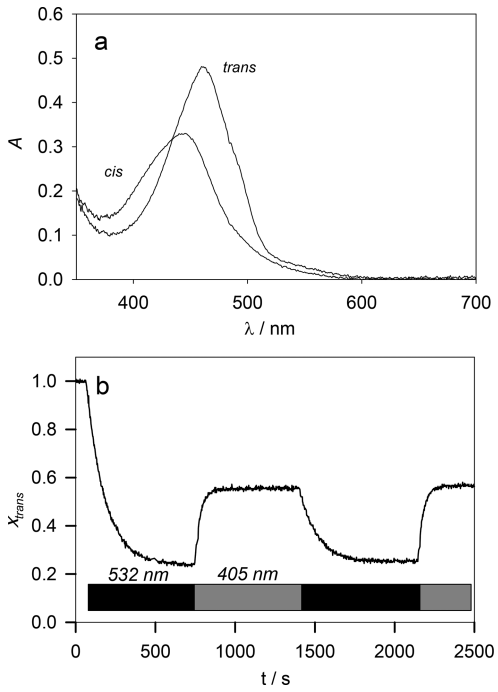

Figure 3. (a) Absorption spectra of *cis*- and *trans*-$[Ru(bpy)_2(PMe_3)(H_2O)]^{2+}$ ([**2**] and [**1**]). (b) Photoconversion between isomers by irradiation with different wavelengths.

Supporting information, Figure S15) yields $\Delta H^{\ddagger}$ = 118 kJ/mol and $\Delta S^{\ddagger}$ = 50 kJ/mol, suggesting a dissociative path for the isomerization process. (see Figure S15 in the Supporting Information)

In order to understand the differences and similarities of the isomers of $[Ru(bpy)_2(PMe_3)(H_2O)]^{2+}$, several simulations based in DFT were performed.

Ground-State DFT Analysis. DFT has been employed to explore the electronic properties of the compounds described in this work. The calculations lead to two stationary points corresponding to the hexacoordinated *cis* and *trans* isomers, with the latter lying ca. 39 kJ mol^{-1} higher in energy. This value explains the impossibility of accessing the trans species by thermal means and suggests that, in the absence of kinetic restrictions, *trans* to *cis* interconversion is strongly favored. The optimized geometry of *cis*-$[Ru(bpy)_2(PMe_3)(H_2O)]^{2+}$ (Figure 4) shows the presence of an Ru^{2+} ion in a distorted-octahedral coordination environment. As is usual at this level of theory, the Ru−N, Ru−O, and Ru−P bond lengths are consistently longer than those observed experimentally in related compounds, for which there are numerous examples. Structural parameters are overall consistent with other reports involving the same computational methodology. The same can be said for the *trans* species, even though very few examples of structurally characterized trans compounds based on the $\{Ru(bpy)_2\}^{2+}$ core have been reported.[24,26] Table S7 in the Supporting Information summarizes relevant structural information for both species.

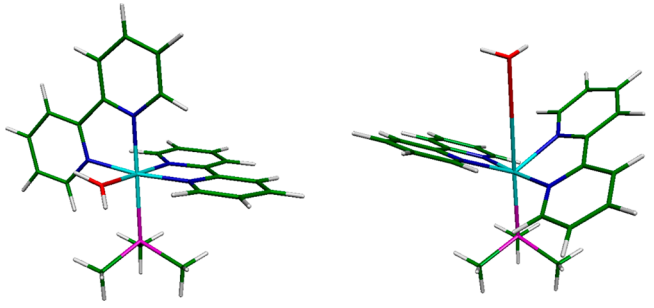

Figure 4. Optimized geometries (DFT) for *cis*-$[Ru(bpy)_2(PMe_3)(H_2O)]^{2+}$ ([**2**]) (left) and *trans*-$[Ru(bpy)_2(PMe_3)(H_2O)]^{2+}$ ([**1**]) (right.)

The electronic spectrum predicted by (TD)DFT for *cis*-$[Ru(bpy)_2(PMe_3)(H_2O)]^{2+}$ shows very good agreement with the experimental spectrum, as can be seen in Figure 5 (top).

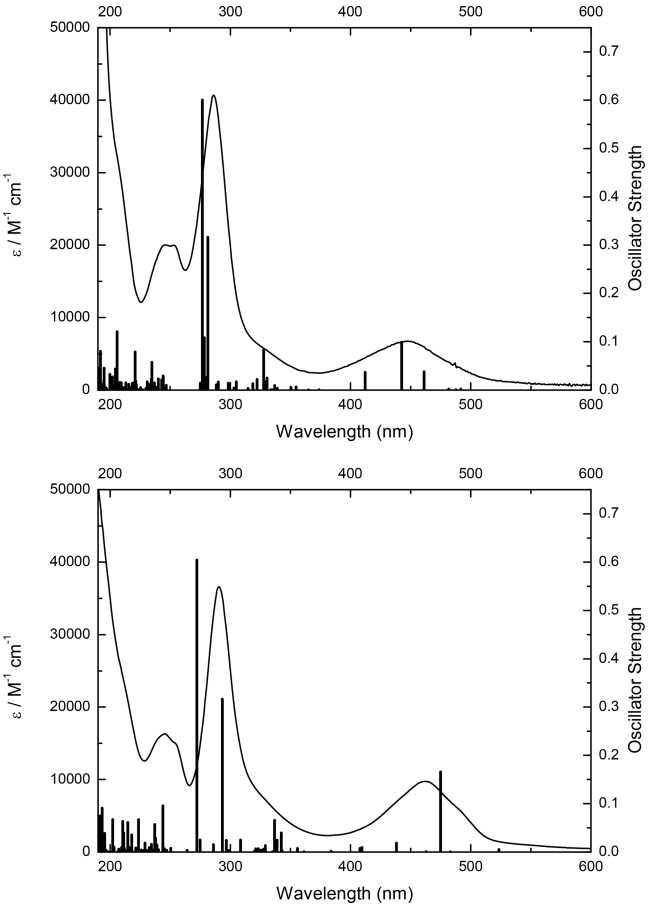

Figure 5. Experimental and computed electronic spectra for *cis*-$[Ru(bpy)_2(PMe_3)(H_2O)]^{2+}$ ([**2**]) (top) and *trans*-$[Ru(bpy)_2(PMe_3)(H_2O)]^{2+}$ ([**1**]) (bottom).

The visible region of the spectrum is dominated by a broad band that can be assigned as MLCT Ru(II)−π^*_{bpy} predicted at 432 nm, in excellent agreement with experimental observations. The same is true for the quality of the predicted electronic spectrum for the *trans* species (Figure 5, bottom), with visible transitions centered at 464 nm also of the MLCT type. At a symmetry lower than octahedral, the degeneration of the t_{2g} orbitals is lifted. In the two cases discussed here, these three orbitals become the molecular orbitals HOMO, H-1, and H-2 of the molecule (see Supporting Information, Figures S16 and S17). These three orbitals are mostly Ru in character for both *cis*-$[Ru(bpy)_2(PMe_3)(H_2O)]^{2+}$ (82%, 85%, and 79% Ru for H, H-1, and H-2, respectively) and *trans*-$[Ru(bpy)_2(PMe_3)(H_2O)]^{2+}$ (82%, 76%, and 92% Ru for H, H-1, and H-2, respectively), the remaining contributions arising mostly from π orbitals of the bpy ligands. On the other hand,

DOI: 10.1021/acs.inorgchem.9b01485
Inorg. Chem. XXXX, XXX, XXX−XXX

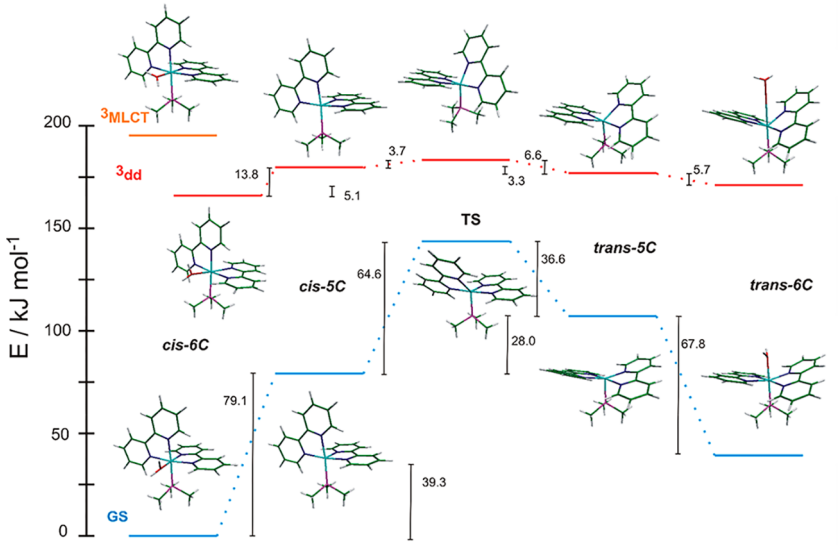

Figure 6. Schematic representation of the reaction coordinate involved in the *cis*−*trans* interconversion over the ground and excited PES. All energies are expressed in kJ mol^{-1}.

the LUMO and LUMO+1 orbitals are bpy-centered (96% and 94% bpy for L and L+1 in the *cis* species and 97% and 94% bpy for L and L+1 in the trans species) and are π^* in nature. In both compounds the MLCT bands result from the convolution of transitions involving the H-1 and H-2 donor orbitals while the L and L+1 MOs behave as acceptors. Transitions involving the HOMO are of very low intensity even when they are symmetry allowed, because of the very poor overlap between the metal and ligand orbitals. Consequently, the lowest energy HOMO−LUMO excited MLCT state contributes only marginally to the experimental absorption profile (see Supporting Information, Tables S8−S11).

Starting from the *trans* species, and always exploring pathways over the ground-state potential energy surface, we found that the thermal interconversion between the isomers proceeds by a three-step mechanism. The most likely pathway connecting the *trans* reagent with the *cis* product seems to involve two intermediate local minima that correspond to pentacoordinated (5C) species due to the dissociation of a water molecule from the stable hexacoordinated (6C) species. The first step involves the elongation of the Ru−O bond, a process that occurs uphill, to allow for the formation of the first 5C intermediate, in which the arrangement of the ligands is reminiscent of that of the 6C reagent. In fact, the Ru−N and Ru−P bond lengths in 5C remain roughly unchanged in comparison to *trans*-6C and the angle between vectors perpendicular to the planes containing the bpy molecules varies only from 32.0° in *trans*-6C to 33.3° in *trans*-5C (Figure 6). The theoretical dissociation energy associated with the process is 67.8 kJ mol^{-1}. The second step is associated with the rotation of one bpy moiety around the Ru−N_3 bond, inducing a change in the relative angle between the bpy molecules, ultimately bringing it to a value of 86.4°, in a conformation of ligands similar to that of the 6C cis product (angle between bpys of 89.4°). The latter is an activated step; the optimization of the first-order saddle point in the trajectory between both 5C species leads to the transition state for the process, with a bipyridine angle of 51.7° and a theoretical activation barrier of 36.6 kJ mol^{-1}. The final step requires the downhill addition of a water molecule to the 5C species to finally yield the more stable 6C cis species.

Excited-State Interconversion. On irradiation in the MLCT transitions located in the visible region, solutions of *cis*-$[Ru(bpy)_2(PMe_3)(H_2O)]^{2+}$ photoisomerize to yield *trans*-$[Ru(bpy)_2(PMe_3)(H_2O)]^{2+}$. At prolonged irradiation times the concentrations of both species become stationary, due to the reversibility of the photoprocess and the simultaneous occurrence of the back thermal reaction. The microscopic sequence involves the following, as already described for the photodetachment of monodentate ligands in Ru-polypyridine complexes. (a) Absorption of light occurs in the visible region to render an excited ^{1}MLCT which relaxes to the lowest energy HOMO−LUMO ^{1}MLCT excited state. (b) Intersystem crossing takes places which leads to a ^{3}MLCT excited state, with this state displaying geometric parameters similar to those in the ground state (see Supporting information, Table S12, Figure S18). (c) The photoactive ^{3}d−d state is thermally populated. The antibonding nature of the newly populated d orbital, which is aligned with the O−Ru−P axis, induces the elongation of the Ru−O bond, to yield a thermalized ^{3}d−d relaxed excited state stabilized 29.3 kJ mol^{-1} with respect to the ^{3}MLCT. The weakening of the Ru−O bond is followed by (d) dissociation of a H_2O molecule to render the ^{3}d−d excited *cis*-5C species. The separation of a water molecule from the coordination sphere is slightly endothermic, involving 10.9 kJ mol^{-1}. Apart from the different coordination number, no significant changes in the bpy conformation are associated with the dissociation process (the bpy molecules lie at 87.1° in *cis*-6C-3dd and 89.5° in *cis*-5C). The rotation of a bpy molecule around the Ru−N_3 bond up to 55.3° allows the conversion between the *cis*- and *trans*-5C forms. The transformation occurs over the lowest energy ^{3}d−d PES and involves a shallow barrier of only 3.7 kJ mol^{-1} to yield the slightly more stable (2.9 kJ mol^{-1}) *trans*-5C isomer. Addition of H_2O to the coordination sphere finally leads to the ^{3}d−d excited state of the *trans*-6C species. As is clear from Figure 6, the overall *cis*−*trans* interconversion over the ^{3}d−d PES involves barriers significantly lower than those in the ground state.

DOI: 10.1021/acs.inorgchem.9b01485
Inorg. Chem. XXXX, XXX, XXX−XXX

Synthetic Applications. One of the central (and often undesirable) aspects in the chemistry of monoaqua complexes of Ru-bpy is the deprotonation of the coordinated water to yield more inert hydroxo complexes at high pH values. The pK_a(cis) of *cis*-$[Ru(bpy)_2(PMe_3)(H_2O)]^{2+}$ is 11.05. We have explored the deprotonation equilibrium in the analogous *trans* complex, which turned to be less acidic (pK_a(trans) = 12.15). This apparently small pK_a difference actually facilitates its use in synthetic procedures, enlarging the pH window to perform ligand change.

Heating of *trans*-$[Ru(bpy)_2(PMe_3)(H_2O)]^{2+}$ in the presence of an L ligand holding a donor N atom, at an appropriate temperature, yields *trans*-$[Ru(bpy)_2(PMe_3)L]^{2+}$. In this way, we have been able to synthesize and isolate the complex *trans*-$[Ru(bpy)_2(PMe_3)ImH]^{2+}$ (ImH = imidazole), which presents a higher quantum yield of photoaquation than its cis isomer. Figure 7 shows a typical photolysis of an aqueous solution of

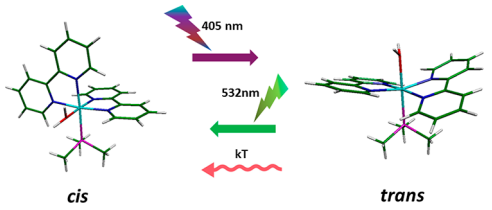

Figure 7. UV−vis spectra of an aqueous solution of *trans*-$[Ru(bpy)_2(PMe_3)ImH]^{2+}$ ([**4**]) during photolysis using a 532 nm laser. Inset: best fit of photoproduct vs irradiation time, for a quantum yield φ_{PD}(trans) = 0.23.

trans-$[Ru(bpy)_2(PMe_3)ImH]^{2+}$. The presence of a neat isosbestic point indicates that the only colored product is the aquo complex. Its *cis*/*trans* ratio will depend on the wavelength used (vide supra).

The inset shows the fitting to a simple model,[7] from which the quantum yield of photolysis can be determined to be $\varphi_{PD}(trans)$ = 0.23, much higher than the corresponding QY for the cis sibling $\varphi_{PD}(cis)$ = 0.10. The visible region MLCT bands of the *trans* species are red-shifted in comparison with their *cis* analogues. Among *cis* complexes with similar structure, lower MLCT energies correlate with lower photodissociation quantum yields. However, this correlation cannot be extended to the comparison between *trans* and *cis* isomers: a systematically higher photodissociation efficiency was found for the studied *trans* complexes, regardless of their red-shifted absorption. The photolysis of the *trans* complexes yields pure ligands in a similar way as for *cis* forms, with no detected side reactions.

We were also able to synthesize *trans* complexes even in cases where we failed to synthesize the corresponding *cis* forms. The reaction between *trans*-$[Ru(bpy)_2(PMe_3)(H_2O)]^{2+}$ and PPh_3 yields *trans*-$[Ru(bpy)_2(PMe_3)(PPh_3)]^{2+}$ in pure form. The corresponding complexes with *cis*-$[Ru(bpy)_2(PPh_3)L]^{2+}$ structure have been widely studied.[7b,27] It is a well-established fact that in these complexes the irradiation on the ^{1}MLCT band is always followed by photorelease of the ligand L, while the phosphine remains coordinated to the Ru center. Conversely, photolysis of *trans*-$[Ru(bpy)_2(PMe_3)(PPh_3)]^{2+}$ yields free PPh_3 and $[Ru(bpy)_2(PMe_3)(H_2O)]^{2+}$, probably due to the higher basicity of PMe_3 (see Figure S19 in the Supporting Information). Unluckily, as *cis*-$[Ru(bpy)_2(PMe_3)(PPh_3)]^{2+}$ could not be synthesized, a comparison of their properties was not possible. Another complex that presents an interesting property is the symmetric *trans*-$[Ru(bpy)_2(PMe_3)_2]^{2+}$, which is very stable both thermally and photochemically. Once more, its *cis* isomer could not be synthesized following the standard procedures.

CONCLUSIONS

We have synthesized for the first time the *trans* isomers of the $[Ru(bpy)_2(PMe_3)(H_2O)]^{2+}$ form. The reaction, which involves an isomerization in the excited state reached by light absorption, was rationalized by employing DFT calculations. We showed that, although the trans isomer can revert to the *cis* form, it is stable enough in solid form and even in aqueous solutions, allowing ligand exchange and photorelease studies and further synthetic uses in a direct, clean way.

Both *cis*- and *trans*-$[Ru(bpy)_2(PMe_3)(H_2O)]^{2+}$ undergo photoisomerization under ^{1}MLCT irradiation. In water solution a photostationary state is reached, which mainly depends on the irradiation wavelength, due to the red-shifted absorption of the *trans* form. Interestingly, while among *cis* isomers a red-shifted ^{1}MLCT band is usually linked to a lower photolysis quantum yield, the *trans* isomers present simultaneously a lower energy ^{1}MLCT and a higher quantum yield. This fact could be useful in devising efficient red-shifted phototriggers. Complexes bearing two phosphines were also synthesized, although it was not possible to produce their *cis* isomers in a similar way. While the heteroleptic PMe_3-PPh_3 complex delivers PPh_3 under visible irradiation, the complex having two PMe_3 groups did not present an appreciable photochemistry.

ASSOCIATED CONTENT

Supporting Information

The Supporting Information is available free of charge on the ACS Publications website at DOI: 10.1021/acs.inorgchem.9b01485.

Mass spectrometric, NMR, and UV−vis characterization of the compounds, complementary computational details and results, and time evolution of *trans*-$[Ru(bpy)_2(PMe_3)(PPh_3)]^{2+}$ irradiated at 525 nm as monitored by NMR (PDF)

AUTHOR INFORMATION

Corresponding Authors

*E-mail for L.D.S.: slep@qi.fcen.uba.ar.

*E-mail for R.E.: rober@qi.fcen.uba.ar.

ORCID

Leonardo D. Slep: 0000-0001-6447-2216

Roberto Etchenique: 0000-0002-5485-8710

Notes

The authors declare no competing financial interest.

ACKNOWLEDGMENTS

The authors thank the University of Buenos Aires, CONICET, and ANPCyT for their financial assistance to conduct the research. R.E. and L.D.S. are members of the scientific staff of CONICET.

REFERENCES

(1) Pinnick, D. V.; Durham, B. Photosubstitution reactions of $Ru(bpy)_2XY^{n+}$ complexes. *Inorg. Chem.* **1984**, *23*, 1440−1445.

DOI: 10.1021/acs.inorgchem.9b01485
Inorg. Chem. XXXX, XXX, XXX−XXX

(2) Durham, B.; Walsh, J. L.; Carter, C. L.; Meyer, T. J. Synthetic applications of photosubstitution reactions of poly(pyridyl) complexes of ruthenium(II). *Inorg. Chem.* **1980**, *19*, 860−865.
(3) Zayat, L.; Calero, C.; Albores, P.; Baraldo, L.; Etchenique, R. A new strategy for neurochemical photodelivery: Metal-ligand heterolytic cleavage. *J. Am. Chem. Soc.* **2003**, *125*, 882−883.
(4) Müller, M.; Dierkes, P. W.; Schlue, W.-R. Ionic mechanism of 4-aminopyridine action on leech neuropile glial cells. *Brain Res.* **1999**, *826*, 63−73.
(5) Nikolenko, V.; Yuste, R.; Zayat, L.; Baraldo, L. M.; Etchenique, R. Two-photon uncaging of neurochemicals using inorganic metal complexes. *Chem. Commun.* **2005**, 1752−1754.
(6) Salierno, M.; Marceca, E.; Peterka, D. S.; Yuste, R.; Etchenique, R. A fast ruthenium polypyridine cage complex photoreleases glutamate with visible or IR light in one and two photon regimes. *J. Inorg. Biochem.* **2010**, *104*, 418−422.
(7) (a) Filevich, O.; Etchenique, R. RuBiGABA-2: a hydrophilic caged GABA with long wavelength sensitivity. *Photochem. Photobiol. Sci.* **2013**, *12*, 1565−1570. (b) Zayat, L.; Noval, M. G.; Campi, J.; Calero, C. I.; Calvo, D. J.; Etchenique, R. A new inorganic photolabile protecting group for highly efficient visible light GABA uncaging. *ChemBioChem* **2007**, *8*, 2035−2038.
(8) Filevich, O.; Salierno, M.; Etchenique, R. A caged nicotine with nanosecond range kinetics and visible light sensitivity. *J. Inorg. Biochem.* **2010**, *104*, 1248−1251.
(9) Cabrera, R.; Filevich, O.; García-Acosta, B.; Athilingam, J.; Bender, K. J.; Poskanzer, K. E.; Etchenique, R. A visible-light-sensitive caged serotonin. *ACS Chem. Neurosci.* **2017**, *8*, 1036−1042.
(10) Araya, R.; Andino-Pavlovsky, V.; Yuste, R.; Etchenique, R. Two-Photon Optical Interrogation of Individual Dendritic Spines with Caged Dopamine. *ACS Chem. Neurosci.* **2013**, *4*, 1163−1167.
(11) (a) Garner, R. N.; Gallucci, J. C.; Dunbar, K. R.; Turro, C. $[Ru(bpy)_2(5\text{-cyanouracil})_2]^{2+}$ as a Potential Light-Activated Dual-Action Therapeutic Agent. *Inorg. Chem.* **2011**, *50*, 9213−9215. (b) Knoll, J. D.; Turro, C. Control and utilization of ruthenium and rhodium metal complex excited states for photoactivated cancer therapy. *Coord. Chem. Rev.* **2015**, *282*−*283*, 110−126. (c) Respondek, T.; Garner, R. N.; Herroon, M. K.; Podgorski, I.; Turro, C.; Kodanko, J. J. Light Activation of a Cysteine Protease Inhibitor: Caging of a Peptidomimetic Nitrile with $RuII(bpy)_2$. *J. Am. Chem. Soc.* **2011**, *133*, 17164−17167.
(12) (a) da Rocha, Z. N.; Marchesi, M. S. P.; Molin, J. C.; Lunardi, C. N.; Miranda, K. M.; Bendhack, L. M.; Ford, P. C.; da Silva, R. S. The inducing NO-vasodilation by chemical reduction of coordinated nitrite ion in *cis*-$[Ru(NO_2)L(bpy)_2]^+$ complex. *Dalton Trans* **2008**, 4282−4287. (b) Franco, L. P.; Cicillini, S. A.; Biazzotto, J. C.; Schiavon, M. A.; Mikhailovsky, A.; Burks, P.; Garcia, J.; Ford, P. C.; Silva, R. S. d. Photoreactivity of a Quantum Dot-Ruthenium Nitrosyl Conjugate. *J. Phys. Chem. A* **2014**, *118*, 12184−12191. (c) Levin, N.; Osa Codesido, N.; Bill, E.; Weyhermuller, T.; Segantin Faspari, A. P.; da Silva, R. S.; Olabe, J. A.; Slep, L. D. Structural, Spectroscopic, and Photochemical Investigation of an Octahedral NO-Releasing $\{RuNO\}^7$. *Inorg. Chem.* **2016**, *55*, 7808−7810.
(13) (a) Salassa, L.; Garino, C.; Salassa, G.; Gobetto, R.; Nervi, C. Mechanism of Ligand Photodissociation in Photoactivable $[Ru(bpy)_2L_2]^{2+}$. Complexes: A Density Functional Theory Study. *J. Am. Chem. Soc.* **2008**, *130*, 9590−9597. (b) Salassa, L.; Borfecchia, E.; Ruiu, T.; Garino, C.; Gianolio, D.; Gobetto, R.; Sadler, P. J.; Cammarata, M.; Wulff, M.; Lamberti, C. Photo-Induced Pyridine Substitution in *cis*-$[Ru(bpy)_2(py)_2]Cl_2$: A Snapshot by Time-Resolved X-ray Solution Scattering. *Inorg. Chem.* **2010**, *49*, 11240−11248.
(14) Word, T. A.; Karolak, A.; Cioce, C. R.; Van Der Vaart, A.; Larsen, R. W. Using Photoacoustic Calorimetry to Study the cis to trans Photoisomerization of the $[Ru(II)(2,2'\text{-bipyridine})_2(H_2O)_2]^{2+}$. Complex in Aqueous Solution. *Comments Inorg. Chem.* **2016**, *36*, 343−354.
(15) Ali, B. A.; Allam, N. K. Propping the optical and electronic properties of potential photo-sensitizers with different π-spacers: TD-DFT insights. *Spectrochim. Acta, Part A* **2018**, *188*, 237−243.
(16) Rojas Pérez, Y.; Etchenique, R. Optical manipulation of animal behavior using a ruthenium-based phototrigger. *Photochem. Photobiol. Sci.* **2019**, *18*, 208−212.
(17) Frisch, M. J. *Gaussian 09, Rev. A.02*; Gaussian Inc., Wallingford, CT, 2009.
(18) (a) Becke, A. D. Density functional calculations of molecular bond energies. *J. Chem. Phys.* **1986**, *84*, 4524−4529. (b) Becke, A. D. Density-functional thermochemistry. III. The role of exact exchange. *J. Chem. Phys.* **1993**, *98*, 5648−5652. (c) Lee, C.; Yang, W.; Parr, R. G. Development of the Colle-Salvetti correlation-energy formula into a functional of the electron density. *Phys. Rev. B: Condens. Matter Mater. Phys.* **1988**, *37*, 785−789. (d) Perdew, J. P. Density-functional approximation for the correlation energy of the inhomogeneous electron gas. *Phys. Rev. B: Condens. Matter Mater. Phys.* **1986**, *33*, 8822−8824.
(19) (a) Dunning, T. H., Jr.; Hay, P. J. In *Modern Theoretical Chemistry*; Schaefer, H. F., III, Ed.; Plenum: New York, 1976; pp 1−28. (b) Hay, P. J.; Wadt, W. R. Ab initio effective core potentials for molecular calculations. Potentials for the transition metal atoms Sc to Hg. *J. Chem. Phys.* **1985**, *82*, 270−283. (c) Hay, P. J.; Wadt, W. R. Ab initio effective core potentials for molecular calculations. Potentials for K to Au including the outermost core orbitals. *J. Chem. Phys.* **1985**, *82*, 299−310. (d) Wadt, W. R.; Hay, P. J. Ab initio effective core potentials for molecular calculations. Potentials for main group elements Na to Bi. *J. Chem. Phys.* **1985**, *82*, 284−298.
(20) (a) Videla, M.; Jacinto, J. S.; Baggio, R.; Garland, M. T.; Singh, P.; Kaim, W.; Slep, L. D.; Olabe, J. A. New Ruthenium Nitrosyl Complexes with Tris(1-pyrazolyl)methane (tpm) and 2,2′-Bipyridine (bpy) Coligands. Structure, Spectroscopy, and Electrophilic and Nucleophilic Reactivities of Bound Nitrosyl. *Inorg. Chem.* **2006**, *45*, 8608−8617. (b) Carrone, G.; Zayat, L.; Slep, L. D.; Etchenique, R. Transient photocyclization in ruthenium(II) polypyridine complexes of indolamines. *Phys. Chem. Chem. Phys.* **2017**, *19*, 2140−2147. (c) De Candia, A. G.; Marcolongo, J. P.; Etchenique, R.; Slep, L. D. Widely Differing Photochemical Behavior in Related Octahedral $\{Ru-NO\}^6$Compounds: Intramolecular Redox Isomerism of the Excited State Controlling the Photodelivery of NO. *Inorg. Chem.* **2010**, *49*, 6925−6930. (d) Petroni, A.; Slep, L. D.; Etchenique, R. Ruthenium-(II) 2,2′-Bipyridyl Tetrakis Acetonitrile Undergoes Selective Axial Photocleavage. *Inorg. Chem.* **2008**, *47*, 951−956. (e) Levin, N.; Osa Codesido, N.; Marcolongo, J. P.; Weyhermueller, T.; Olabe, J. A.; Slep, L. D. Remarkable changes of acidity of bound nitroxyl (HNO) in the $[Ru(Me_3[9]aneN_3)(L^2)(NO)]^{n+}$ family (n = 1−3). Systematic structural and chemical exploration and bioinorganic chemistry implications. *Inorg. Chem.* **2018**, *57*, 12270−12281.
(21) Videla, M.; Roncaroli, F.; Slep, L. D.; Olabe, J. A. Reactivity of Reduced Nitroprusside, $[Fe(CN)_5NO\bullet]^{3-}$, toward Oxygen. *J. Am. Chem. Soc.* **2007**, *129*, 278−279.
(22) Peng, C.; Bernhard Schlegel, H. Combining Synchronous Transit and Quasi-Newton Methods to Find Transition States. *Isr. J. Chem.* **1993**, *33*, 449−454.
(23) (a) Fukui, K. Formulation of the reaction coordinate. *J. Phys. Chem.* **1970**, *74*, 4161−4163. (b) Fukui, K. The path of chemical reactions - the IRC approach. *Acc. Chem. Res.* **1981**, *14*, 363−368. (c) Maeda, S.; Harabuchi, Y.; Ono, Y.; Taketsugu, T.; Morokuma, K. Intrinsic reaction coordinate: Calculation, bifurcation, and automated search. *Int. J. Quantum Chem.* **2015**, *115*, 258−269.
(24) Durham, B.; Wilson, S. R.; Hodgson, D. J.; Meyer, T. J. *Cis-trans* photoisomerization in $Ru(bpy)_2(OH_2)_2^{2+}$. Crystal structure of trans-$[Ru(bpy)_2(OH_2)(OH)](ClO_4)_2$. *J. Am. Chem. Soc.* **1980**, *102*, 600−607.
(25) Walsh, J. L.; Durham, B. *Trans* isomers of ruthenium(II) complexes containing two bipyridine ligands. *Inorg. Chem.* **1982**, *21*, 329−332.
(26) (a) Cordes, A. W.; Durham, B.; Swepston, P. N.; Pennington, W. T.; Condren, S. M.; Jensen, R.; Walsh, J. L. Structural chemistry of

DOI: 10.1021/acs.inorgchem.9b01485
Inorg. Chem. XXXX, XXX, XXX−XXX

necessarily distorted bis(bipyridine) complexes. The crystal structure of the *trans*-[bis(2,2′-bipyridine)bis(triphenyl-phosphine)ruthenium-(ii)] and *trans*-[bis(4,4′-dimethyl-2,2′-bipyridine)bis(pyridine)-ruthenium(II)] cations. *J. Coord. Chem.* **1982**, *11*, 251−260. (b) Blake, A. J.; Marr, A. M.; Rankin, D. W. H.; Schroder, M. Structure of *trans*-[bis(2,2′-bipyridyl)bis(methyldiphenylphosphine)-ruthenium(II)] perchlorate tetrahydrofuran solvate. *Acta Crystallogr., Sect. C: Cryst. Struct. Commun.* **1988**, *44*, 935−936. (c) Nagao, H.; Nishimura, H.; Funato, H.; Ichikawa, Y.; Howell, F. S.; Mukaida, M.; Kakihana, H. Synthesis, properties, and molecular structure of *trans*-chloro(nitrosyl)bis(2,2′-bipyridine)ruthenium(2+): trans and cis isomer characteristics compared. *Inorg. Chem.* **1989**, *28*, 3955−3959. (d) Togano, T.; Kuroda, H.; Nagao, N.; Maekawa, Y.; Nishimura, H.; Howell, F. S.; Mukaida, M. Synthesis, properties and molecular structure of *trans*-hydroxobis(2, 2′-bipyridine)-nitrosylruthenium(2+): influence of axial ligand on characteristics of nitrosyl moiety in trans-$[Ru(NO)XL_4]^{n+}$ (X = OH, Cl; L = py, 1/2(bpy)) type complexes. *Inorg. Chim. Acta* **1992**, *196*, 57−63. (e) Cordes, A. W.; Durham, B.; Pennington, W. T. Crystal and molecular structures of trans-bis(acetonitrile)bis(bipyridine)-ruthenium(II) perchlorate and trans-diamminebis(bipyridine)-ruthenium(II) perchlorate. *J. Crystallogr. Spectrosc. Res.* **1992**, *22*, 699−704. (f) Weathers, N. R.; Sadoski, R. C.; Durham, B.; Cordes, A. W. *trans*-Diaquabis(2,2′-bipyridine-N,N′)ruthenium(II) Bis-(hexafluorophosphate). *Acta Crystallogr., Sect. C: Cryst. Struct. Commun.* **1997**, *53*, 1047−1049. (g) Klufers, P.; Zangl, A. *trans*-bis (2,2′-bipyridine)dichloridoruthenium(II). *Acta Crystallogr., Sect. E: Struct. Rep. Online* **2007**, *63*, No. m3088. (h) Jude, H.; White, P. S.; Dattelbaum, D. M.; Rocha, R. C. *trans*-Diaquabis(2,2′-bipyridine-[kappa]^{2}N,N′)ruthenium(II)bis(trifluoromethanesulfonate). *Acta Crystallogr., Sect. E: Struct. Rep. Online* **2008**, *64*, m1388−m1389. (i) Haghighi, F. H.; Hadadzadeh, H.; Farrokhpour, H.; Serri, N.; Abdi, K.; Amiri Rudbari, H. Computational and experimental study on the electrocatalytic reduction of CO_2 to CO by a new mononuclear ruthenium(II) complex. *Dalton Trans* **2014**, *43*, 11317−11332.

(27) (a) Sullivan, B. P.; Salmon, D. J.; Meyer, T. J. Mixed phosphine 2,2′-bipyridine complexes of ruthenium. *Inorg. Chem.* **1978**, *17*, 3334−3341. (b) Litke, S. V.; Ershov, A. Y. Photophysics of bis-bipyridyl complexes of ruthenium(II) with triphenylphosphine. *Opt. Spectrosc.* **2011**, *110*, 522.

DOI: 10.1021/acs.inorgchem.9b01485
Inorg. Chem. XXXX, XXX, XXX−XXX